ORIGINAL PAPER

Sensitivity analysis of convective and PBL parameterization schemes for Luban and Titli tropical cyclones

Saurabh Verma[1] · Subodh Kumar[2] · Sunny Kant[3] · Sanchit Mehta[4]

Abstract

Tropical cyclones (TCs) are the most distractive natural weather phenomena and cause extensive damage and socioeconomic loss over the North Indian Ocean (NIO) region. Convection and planetary boundary layer (PBL) system play a vital role in the origin and strengthening of the TCs. The various convective and PBL parameterization schemes are available in the statistical model, which integrates these processes. The efficient incorporation of these schemes is vital to enhance the performance of the numerical weather prediction (NWP) model. In the present study, twelve experiments have been designed to carry out the numerical simulations using Advance Research Weather Research and Forecasting (ARW) model. The behavior and performance of the schemes have been evaluated to verify the instantaneous forecast of the TCs. The simulated cyclone track, which is assessed with the Indian Meteorological Department (IMD) best track data, indicates that the vector displacement error and RMSE for the experiment MWBM and YWBM are < 100 km and < 10 km, respectively. The maximum sustained 10-m wind prediction shows MWKF for Luban and YWKF for Titli have the least RMSE value, accounting for 7.13 ms^{-1} and 9.75 ms^{-1}. The equitable threat score (ETS) at 24-h accumulated rainfall is > 0.4 for MLBM and up to 60 mm in Luban. However, it is > 0.6 for YLBM and up to 40 mm for Titli. Based on the results and keeping the cyclone track, intensity, and rainfall, the BMJ convective scheme with the YSU and MYJ PBL has better predicting skills over the NIO region. The KF scheme has better skills in the prediction of TC intensity.

1 Introduction

Tropical cyclones (TCs) are rapidly spinning and most significant natural hazardous systems that carry high wind speeds and rainfall (Mohanty et al. 2012; Mohapatra et al. 2015). They are generally characterized by a low-pressure center developed over a warm ocean region and intensified under favorable prevailing meteorological conditions. Warm ocean transports more energy to the atmosphere in the form of sensible and latent heat, which supports the creation of a low-pressure rotating frame via key atmospheric thermodynamics related to low-level dynamical convergence, which contributes to the intensification of the surface low to cyclonic storms (Rao and Prasad 2007).

The TCs are mainly developed throughout the pre-monsoon and post-monsoon seasons. The nearby existence of an equatorial trough over the NIO may account for a seasonal incidence of TCs in the open ocean (Ramage 1974; Vishnu et al. 2019). Among the world's oceans, the NIO, which includes the Arabian Sea (AS) and the Bay of Bengal (BOB), is a highly active area for the growth of TCs (Balaji et al. 2018) and is responsible for 7% of all TC formations worldwide (WMO 2014). TCs significantly impact the loss of the human race, physical property, ecosystem, and environment at different levels. Therefore, accurate forecasting of cyclone tracks, intensity, and landfall is critical for reducing socioeconomic risks. According to some previous studies, the track prediction has been enhanced due to consideration of new parameterization schemes in the advanced numerical modeling and up-gradation in the data assimilation technique (Mohanty and Gupta 1997; Rao and Bhaskar Rao 2003; Mandal et al. 2004; Mohanty et al. 2019; Mohan et al. 2019). However, intensity forecasts remain a complex

✉ Sanchit Mehta
  mehta.sanchit@gmail.com

[1] Department of Marine and Atmospheric Sciences, Indian Institute of Remote Sensing, ISRO, Dehradun, India

[2] Molecular and Atmospheric Spectrometry Group (GSMA), University of Reims Champagne-Ardenne, Reims, France

[3] Center of Atmospheric Sciences, Indian Institute of Technology, Delhi, New Delhi, India

[4] University of Miami Rosenstiel School of Marine and Atmospheric Science, Miami, FL, USA

problem (Bender and Ginis 2000; Knaff et al. 2003; Krishnamurti et al. 2005; De Maria et al. 2005; Rogers et al. 2006) and still lag behind improvements in track prediction.

Furthermore, the modeling approach has been carried out by several studies using the ARW model to evaluate the influence of physical parameterization schemes for forecasting TC track and intensity (Raju et al. 2011; Pattanayak et al. 2012; Deshpande et al. 2012; Chandrasekar and Balaji 2012). The convective process and PBL dynamics play an essential role in the genesis and intensification of TCs among all schemes examined in the WRF-ARW model. However, microphysical parameterization has a considerable impact on TC track prediction (Raju et al. 2011; Chandrasekar and Balaji 2012). Using the ARW model, the TC track, intensity, and rainfall along with Kain–Fritsch (KF) convective and Yonsei University (YSU) PBL schemes are well simulated for TC Gonu (Osuri et al. 2012, 2013). Kanase and Salvekar (2015) show that the Bettes-Miller-Janjic (BMJ) combined with the YSU PBL scheme replicated improved results for the TC Laila. However, Sun et al. (2014) found a well-simulated TC track with the combination of Grell-Devenyi (GD) convective and Mellor-Yamada-Janjic (MYJ) PBL. The outcomes from previous studies using the Non-Hydrostatic Mesoscale Model (NMM) with the combination of KF convective parameterization scheme (CPS) and YSU PBL to forecast track and strength for TC Gonu, Sidr, and Nargis were not really adequate (Srinivas et al. 2013; Mohandas and Ashrit 2014).

From the studies mentioned above, it is still challenging to identify an appropriate convective and PBL parameterization scheme to predict the TCs over the NIO basin. In this present study, the numerical simulations have been carried out using ARW model version 3 with three convective, two PBL, and two microphysical parameterization schemes over the NIO basin. This study aims to evaluate an appropriate physical parametrization scheme within the model for the numerical simulations of TCs (to predict the track, intensity, and landfall). This assessment analysis will help to improve the operational model setup for productive use in TCs forecast.

1.1 TC case description

Since 1977, this is the first time when two very severe cyclones Luban and Titli came simultaneously to the NIO region. The cyclonic storm Luban had activated in the AS and did not affect any coast of India, while Titli had activated in BOB and was forecasted to hit the coasts of Odisha and North Andhra Pradesh. The genesis of both TCs started when the disturbance began in the open ocean as a result of the active Inter Tropical Convergence Zone (ITCZ) has begun to move southward toward the coast. Both cyclones had in common the pre-conditioning of the

upper ocean in 2018 due to the co-occurrence of El Niño, the positive phase of the Indian Ocean dipole, and the cold phase of the Pacific decadal oscillation, all of which worked in tandem to warm the AS and sections of the BOB. The advent of the Madden–Julian oscillation (MJO) and the mixed Rossby-gravity wave during the first week of October caused the emergence of Luban in the AS. The eastward propagation of the MJO and the associated enhanced convection from the AS toward the region of origin of Titli, together with the arrival of the downwelling oceanic Rossby wave, prompted the birth of Titli in the BOB (Chowdhury et al. 2021; Srivastava et al. 2021).

1.2 Luban

According to the IMD report (2018), Luban was the third TC that goes up to the very severe cyclonic storm (VSCS) stage over the NIO region in 2018. Luban had been activated on 6th October in the central AS and followed a general west-northwestward path for most of its existence.

On October 6th, IMD well recognized the system as being in the depression stage. The depression stage had been upgraded to a deep depression on October 7th. The TC Luban on October 8th was designated as a cyclonic storm (CS) by the IMD classification; when it had swirling rainbands around a robust central thunderstorm region, there was clear outflow to the north. According to Joint Typhoon Warning Center (JTWC), the circulation became more distinct over time, generally steered west-north-westward by a subtropical ridge to its north (JTWC report 2018). Luban was again upgraded to a severe cyclonic storm (SCS) on October 9 by the IMD as thunderstorms started to bloom over the circulation. On October 10th, Luban was further upgraded by IMD to a VSCS, with a maximum sustained wind speed of 33 ms^{-1}, similar to a category 1 hurricane. On the same day, both the IMD and the JTWC projected that Luban would attain a maximum wind speed peak of 39 ms^{-1}. Besides, they also predicted that the storm would remain at its general trajectory and strike the Arabian Peninsula.

On October 13th, Luban signaling re-intensification due to increasing thunderstorm activity. On October 14th, Luban made rainfall around 6 UTC over eastern Yemen, about 30 km south of Al Ghaydah, with a wind speed of 21 ms^{-1}. On October 15th, the storm rapidly dissipated over the dry and mountainous terrain. TC Luban caused flooding in Somalia, Yemen, and Oman. Whereas fourteen people were killed in Yemen when heavy rainfall cut off villages and destroyed roads. In Oman, a small locust outbreak occurred due to desert rainfall, and the entire country's damage was reported to be worth $1 billion.

1.3 Titli

Titli was a deadly and devastating TC that caused a high socioeconomic loss in Eastern India and Bangladesh. The cyclonic storm emerged from low pressure in the Andaman Sea on 6th October 2018 and further moved west-northwestwards.

The depression was well identified by IMD on 8th October 2018 and upgraded to deep depression on October 9th. This was further intensified on October 10th and upgraded to a VSCS phase, and on the Saffir–Simpson scale, it was comparable to a category 3 hurricane. Titli made landfall near Palasa (Andhra Pradesh) and the south coast of Odisha from 2300 to 0000 UTC. Moving further north-northwestwards, it started weakening to an SCS on 11th October and a CS on the same evening. Furthermore, the system started progressing northeastwards under the influence of southwesterly winds from 11 p.m. on 12th October and progressively dissipated into a low-pressure area (LPA) around Gangetic West Bengal and neighboring Bangladesh on the morning of 13th October 2018. Due to heavy rainfall and landslides, it appealed to the lives of many people in Andhra Pradesh, Odisha, and other coastal regions (RSMC report 2019). The model description and methodology are discussed in the "Model description and methodology" section. Detailed information about the data used is discussed in the "Data used" section. The simulated results are discussed in the "Results and discussions" section. The conclusion and findings are discussed in the "Conclusion" section.

2 Model description and methodology

In the present study, we have considered TC Titli (October 8–12, 2018) and Luban (October 6–15, 2018). Both TCs are severe cyclones, and it is infrequent when BOB and AS host cyclonic storms of this strength at the same time. Titli has been developed over the BOB and Luban over the AS in the NIO region. Luban did not affect India's coast, whereas Titli hit the coast of Odisha and adjoining North Andhra Pradesh.

The numerical simulations are carried out using the WRF model version 3 (release 3.9.1). WRF is a non-hydrostatic next-generation mesoscale model with a range of nesting capabilities (Skamarock and Klemp 1992; Wang et al. 2004; Skamarock et al. 2005). The WRF model offers many different physics options to signify cloud properties, solar radiation, precipitation, and surface and boundary layer process. Many previous studies already tested the performance of this WRF version over different oceanic basins and discovered that the model can reasonably predict/simulate tropical storms and rainfall occurrences (Mahala et al. 2019; Hon 2020; Baki et al. 2022; Makar and Pant 2022). Therefore, on previous considerations, this model version has been chosen for a single domain with a spatial resolution of 9 km and 35 vertical levels up to 100 hPa (Fig. 1). Presently, physical parameterization options are comprised in the WRF model (Skamarock et al. 2019), i.e., microphysics, cumulus parameterization, PBL parameterization, longwave and shortwave radiation, surface layer, and land surface parameterization (Gunwani and Mohan 2017). The twelve experiments have been designed using three convective (KF, BMJ, and GD), two PBL (YSU, and MYJ), and two microphysics Lin (Lin et al. 1983) and WDM6 (Rutledge and Hobbs 1984) schemes. The previous studies suggested that the mentioned schemes are the best suitable schemes for the prediction of TC track, intensity, and rainfall (Pattanayak and Mohanty 2008; Mohanty et al. 2010; Osuri et al. 2012 and 2013). Therefore, with the continuation and following the proposed objective of this study, these schemes' combinations have been chosen. Detailed information about the

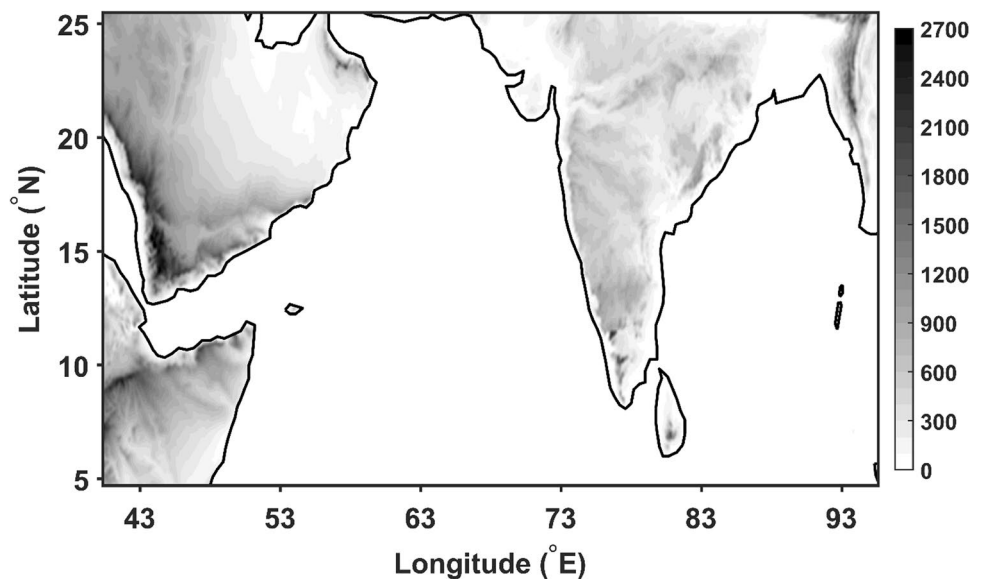**Fig. 1** The topographical map indicates the model domain and terrain height (in meters)

Table 1 The ARW-WRF model configuration parameterization schemes were used in this study

Dynamics	Non-hydrostatics
Simulation duration	264 h
Initial conditions	6 hourly NCEP FNL (1°×1°) data
Domain resolution	9×9 km
Grid points	660×260
Vertical levels	35 terrain-following
Horizontal grid system	Arakawa-C grid
Integration time step	45 s
Time integration scheme	3rd order runga-kutta scheme
Spatial differencing scheme	6th order center differencing
Land surface parametrization	Noah land surface scheme
Shortwave radiation scheme	Dudhia scheme
Longwave radiation scheme	RRTM
PBL scheme	YSU, MYJ
MP scheme	Lin et al., WDM6
Cumulus scheme	Kain-Fritch (KF), Betts-Miller-Janjic (BM), Grell-Devenyi (GD)

Table 2 Experiments are designed for the simulations with the combination of PBL, MP, and Cumulus parameterizations

PBL	MP	Cumulus	Ex. name
YSU	Lin et al	KF	YLKF
YSU	Lin et al	BM	YLBM
YSU	Lin et al	GD	YLGD
MYJ	Lin et al	KF	MLKF
MYJ	Lin et al	BM	MLBM
MYJ	Lin et al	GD	MLGD
YSU	WDM6	KF	YWKF
YSU	WDM6	BM	YWBM
YSU	WDM6	GD	YWGD
MYJ	WDM6	KF	MWKF
MYJ	WDM6	BM	MWBM
MYJ	WDM6	GD	MWGD

model configuration and experiment design is discussed in Tables 1 and 2.

The PBL schemes are different in their closure approach, such as local and nonlocal. The Mellor-Yamada-Janjić (MYJ) is classified as a local 1.5-order turbulence closure scheme (Janjic 1994). MYJ uses turbulent kinetic energy to parameterize eddy diffusivity through local vertical mixing. The Yonsei University (YSU) PBL is typically a nonlocal 1st-order turbulence closure parameterization scheme that uses k-theory to describe the role of turbulence upon the mean variables (Hong and Lim 2006). It is an updated version of the medium-range forecast (MRF) scheme (Hong and Pan 1996). The YSU PBL accompanies an explicit treatment of the entrainment process at the top of the boundary layer and rectifies systematic biases of the large-scale features such as cold bias.

Three convection schemes are tested based on target differing vertical transport strengths. First, Kain and Fritsch (KF) is a shallow and deep convection scheme used for a mass-flux approach to parameterizing both updraft and downdraft (Kain and Fritsch 1993). The mixing is permitted in all vertical levels through entrainment and detrainment processes with the CAPE removal duration. The KF scheme entails a convective triggering function (in light of grid-resolved vertical velocity), closure assumptions, and mass-flux formulation. Second, Betts, Miller, and Janjic (BMJ) is assessed as a convective adjustment scheme rather than mass flux that forces soundings toward the reference profile of specific humidity and temperature at every grid point (Betts and Miller 1986; Janjic 1994). The scheme's structure favors enactment when substantial moisture measures are available in the low- and mid-level with flattering CAPE. Third, Grell and Devenvi (GD) is an ensemble convective parameterization scheme that incorporates several mass-flux cumulus schemes with diverse precipitation efficiencies and updraft and downdraft entrainment as well as detrainment parameters (Grell and Devenyi 2002). Moreover, the dynamic control closure depends upon moisture convergence, CAPE, and low-level vertical velocity.

3 Data used

We have considered the National Center of Environmental Prediction (NCEP) Final (FNL) operational global analysis data at 1°×1° spatial resolution and 6-h temporal resolution for the initial and boundary condition. This item is from the global data assimilation system, which continually gathers observational information from the global telecommunication system (GTS). We have used IMD data to validate intensity, central sea level pressure (CLSP), and cyclone track. GPM data at 0.1°×0.1° spatial resolution and half-hour temporal resolution are used to validate the rainfall distribution.

4 Results and discussions

The prediction of cyclone track, intensity, and landfall is measured as the utmost critical and challenging concern. In contrast, a misplaced forecast of the cyclonic center will produce an approximate location of rainfall and intensification of TCs, which could cause high socioeconomic loss. Therefore, a precise track forecast is significant to spot the physical position where huge damages would be expected due to high wind speed and extreme rainfall. For that purpose, numerical simulations have been carried out using the

ARW model. The statistical errors have been calculated to validate the model outcomes, such as root mean square error (RMSE), mean square error (MSE), normalized mean square error (NMSE), index of agreement (IOA), and standard deviation (SD), as shown in Tables 3 and 4. The performance of schemes on different physical processes is discussed in "Cyclone intensity and track."

4.1 Cyclone intensity and track

The track and intensity prediction of TC by using the combination of three convection (KF, BMJ, and GD) schemes, two PBL (YSU and MYJ), and two microphysics (Lin et al. and WDM 6) schemes are discussed in this section. Figure 2 indicates that the BMJ CPS has better skill in predicting cyclone tracks with the grouping of WDM6 microphysics and MYJ PBL for Luban and YSU PBL for Titli, as compared with the IMD observations. From Fig. 3, the RMSE and vector displacement error (VDE) for the experiment MWBM are respectively < 80 km and < 8 km for TC Luban. For TC Titli, the YWBM VDE and RMSE are around < 100 km and < 10 km. The worse cyclone track is displayed by the

Table 3 Statistical performance indexes of central sea level pressure (CSLP) and 10-m wind speed (WS10m) concerning IMD observations for Luban

	EX	IOA	MSE	SD	NMSE
CSLP (Luban)	**YLKF**	0.61	339.12	16.19	0.000019
	YLBM	0.36	309.44	12.82	0.000017
	YLGD	0.57	**85.76**	**6.99**	**0.000005**
	MLKF	0.54	584.39	20.53	0.000032
	MLBM	0.48	512.55	20.19	0.000028
	MLGD	0.57	194.40	12.41	0.000011
	YWKF	**0.63**	271.27	14.31	0.000015
	YWBM	0.52	154.35	8.63	0.000008
	YWGD	0.58	104.00	8.20	0.000006
	MWKF	0.55	528.41	19.70	0.000029
	MWBM	0.55	169.98	13.36	0.000009
	MWGD	0.54	155.77	10.77	0.000008
WS$_{10m}$ (Luban)	**YLKF**	0.70	64.63	4.94	0.0100
	YLBM	0.47	143.17	3.72	0.0296
	YLGD	0.46	222.66	2.98	0.0884
	MLKF	**0.76**	**50.81**	5.33	**0.0075**
	MLBM	0.62	92.67	4.82	0.0164
	MLGD	0.50	188.90	3.55	0.0636
	YWKF	0.67	72.07	4.67	0.0118
	YWBM	0.49	152.37	**2.82**	0.0370
	YWGD	0.48	210.73	2.89	0.0809
	MWKF	0.74	56.10	5.35	0.0085
	MWBM	0.54	152.05	3.72	0.0391
	MWGD	0.48	195.43	3.47	0.0654

Table 4 Same as Table 3 but for Titli

	EX	IOA	MSE	SD	NMSE
CSLP (Titli)	**YLKF**	0.63	378.08	18.76	0.000036
	YLBM	0.47	172.57	8.86	0.000016
	YLGD	0.29	178.99	3.88	0.000016
	MLKF	0.49	268.62	13.19	0.000025
	MLBM	**0.89**	**77.32**	15.01	**0.000007**
	MLGD	0.44	216.13	**1.97**	0.000019
	YWKF	0.63	371.16	18.84	0.000035
	YWBM	0.76	130.85	11.38	0.000012
	YWGD	0.37	155.07	2.57	0.000014
	MWKF	0.55	292.96	15.04	0.000027
	MWBM	0.73	189.65	15.87	0.000018
	MWGD	0.46	185.43	1.77	0.000017
WS$_{10m}$ (Titli)	**YLKF**	0.65	113.71	6.24	0.0439
	YLBM	0.48	185.87	3.72	0.0986
	YLGD	0.44	286.75	1.66	0.3768
	MLKF	0.56	152.88	4.45	0.0797
	MLBM	0.66	101.03	4.67	0.0445
	MLGD	0.44	331.56	**0.81**	0.6889
	YWKF	**0.71**	**95.06**	6.55	**0.0340**
	YWBM	0.61	116.67	4.56	0.0504
	YWGD	0.45	265.64	1.22	0.2937
	MWKF	0.60	132.73	4.81	0.0648
	MWBM	0.64	114.52	5.24	0.0490
	MWGD	0.44	312.05	1.09	0.5244

GD scheme. When compared to other schemes, the GD scheme's TC track for Titli is expanding substantially after 36 h of projection. As a result, the GD scheme was not chosen for the prediction of either TCs. Furthermore, in terms of predicting cyclone tracks, the KF scheme with the combination of YSU PBL and WDM6 microphysics comes in second. Over the entire forecast period, the VDE for Luban is < 130 km and the RMSE is < 12 km, while the VDE for Titli is < 200 km and the RMSE is < 13 km (see Fig. 3). The findings from the current study indicate reasonable mean track errors as compared to earlier research using simulations from the ARW model (Raju et al. 2011; Osuri et al. 2012 and 2013).

Furthermore, the TC intensity is conferred in the maximum sustained surface wind (MSW) speed and central sea level pressure (CSLP) in Fig. 4. For Luban, the observed least CSLP is around 980 hPa on 10th Oct 2018 at 12:00 UTC; however, for Titli, it is about 972 hPa at the same time (Fig. 4a,c). The results initially show that the BMJ-YSU scheme combination with WDM6 microphysics similarly followed the observation, but after midnight on 10th October, the CSLP was over-predicted. On the other hand, the KF convective with both the PBL MYJ and YSU overestimated the CSLP for the entire time frame.

Fig. 2 The model simulated the TC track for Luban and Titli at 12-h time intervals from different parameterization schemes
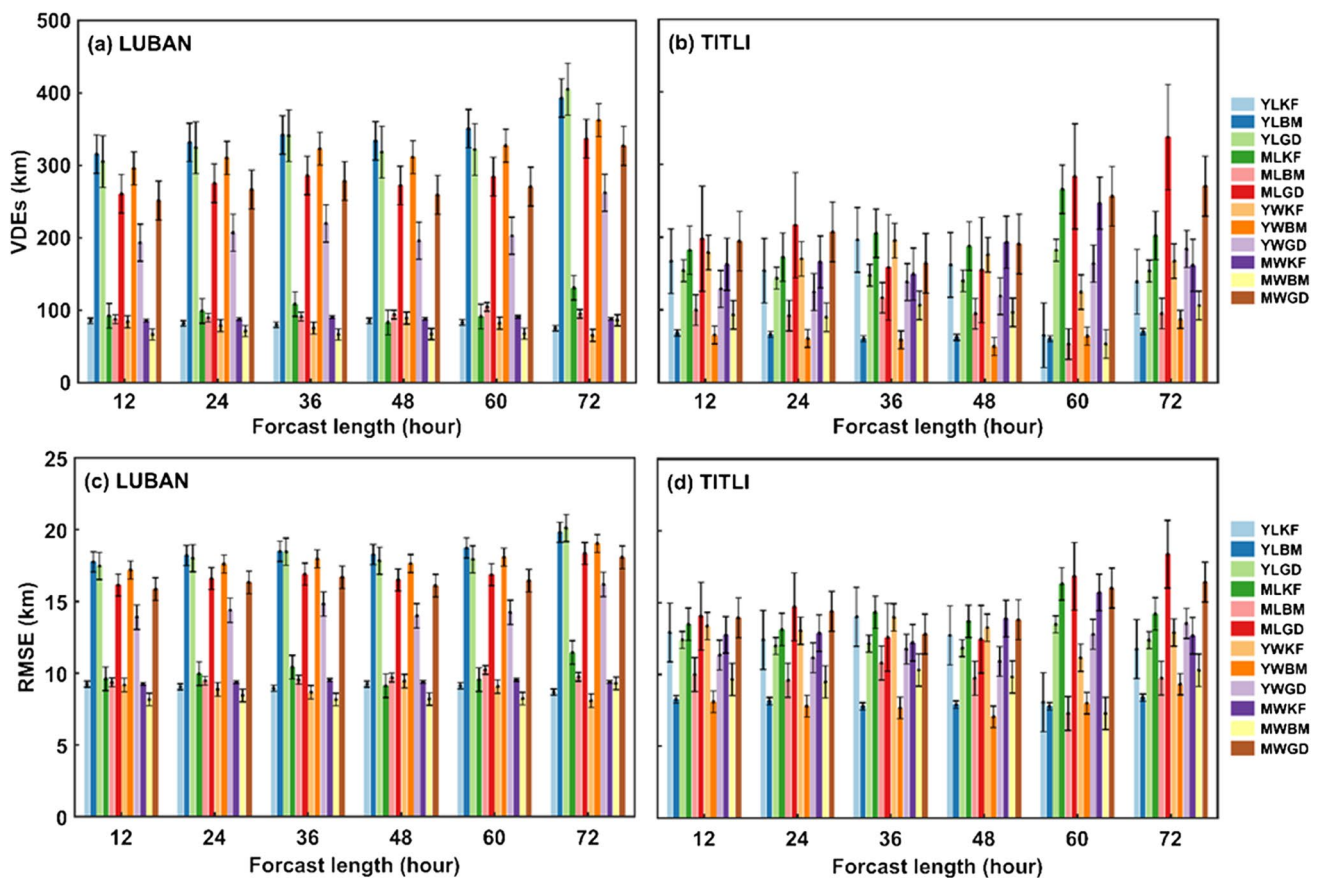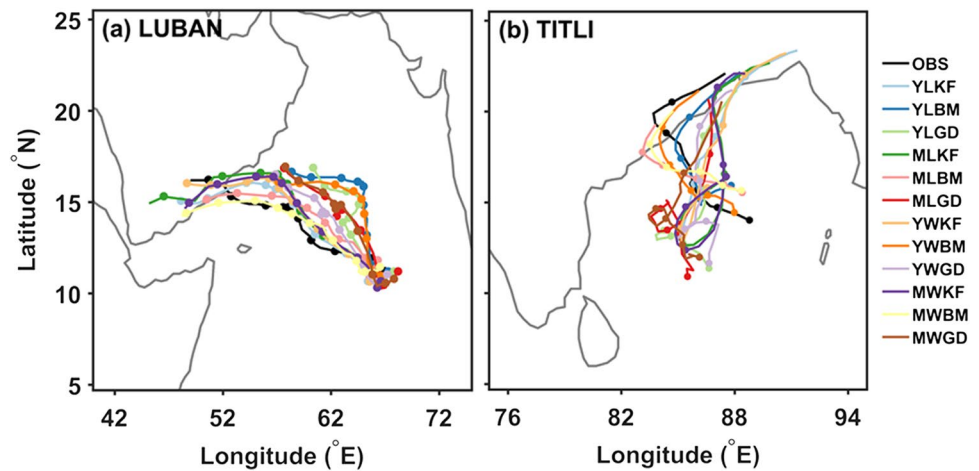

Fig. 3 The vector displacement error (VDEs, km) and root mean square error (RMSE, km) at 12-h time intervals for TC Luban and Titli. Here, the error bar indicates the standard deviation

Figure 5a clearly shows that the CSLP for GD CPS with RMSE value ~ 9.26 hPa is close to the observation with the combination of YSU and Lin et al. scheme for Luban. However, for Titli, the BMJ convective scheme with MYJ PBL has an RMSE value is nearly 8.79 hPa (Fig. 5b). Figure 4b,d illustrates that the above-specified schemes affect the time

series of maximum 10-m wind with the corresponding observations from the IMD. The maximum estimated surface wind is around ~ 38.5 ms^{-1} for Luban and ~ 41 ms^{-1} for Titli at 12:00 UTC on 10th October and 00:00 UTC on 11th October. The experiment MWKF and YWKF simulated maximum sustained surface wind ~ 25 ms^{-1} for Luban
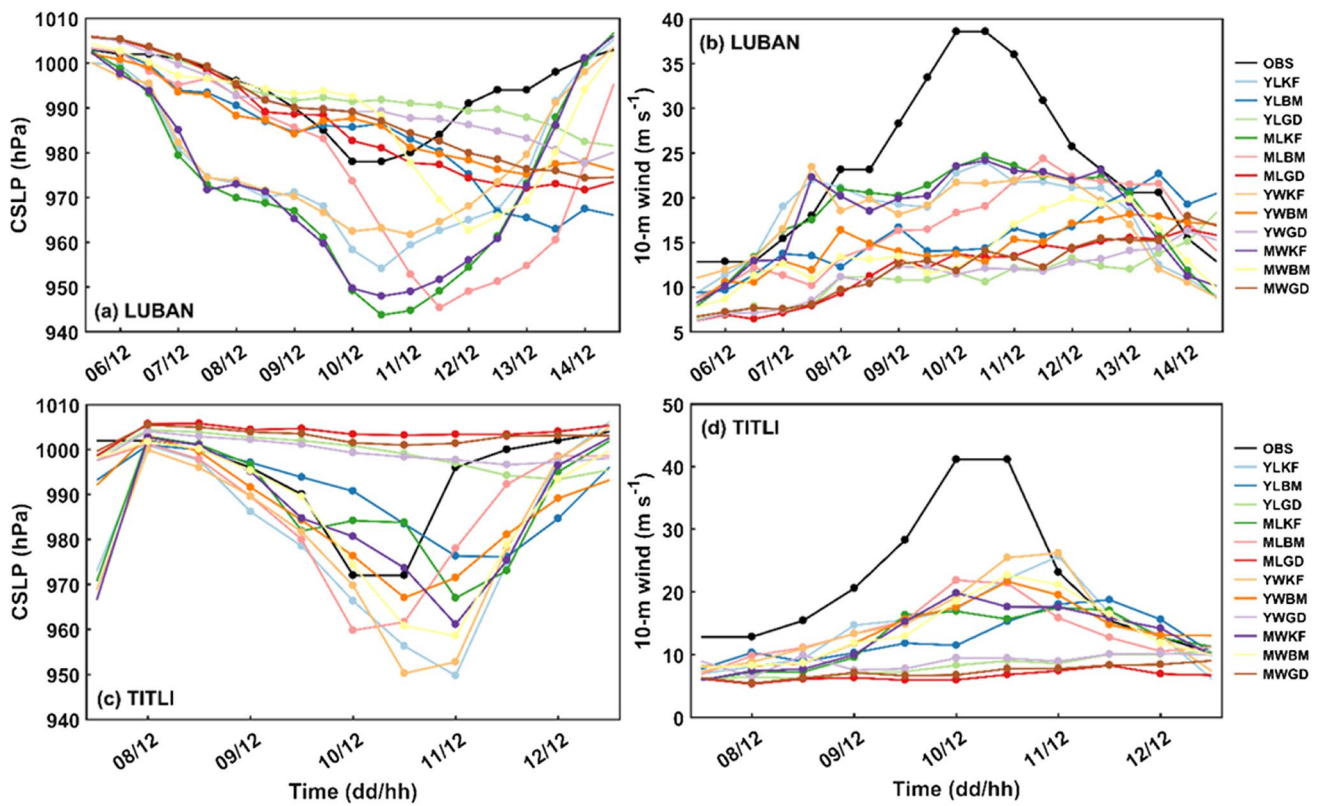
Fig. 4 The time series of predicted TC intensity in terms of central sea level pressure (hPa; **a** and **c**) and 10-m wind speed (ms^{-1}; **b** and **d**) for Luban and Titli
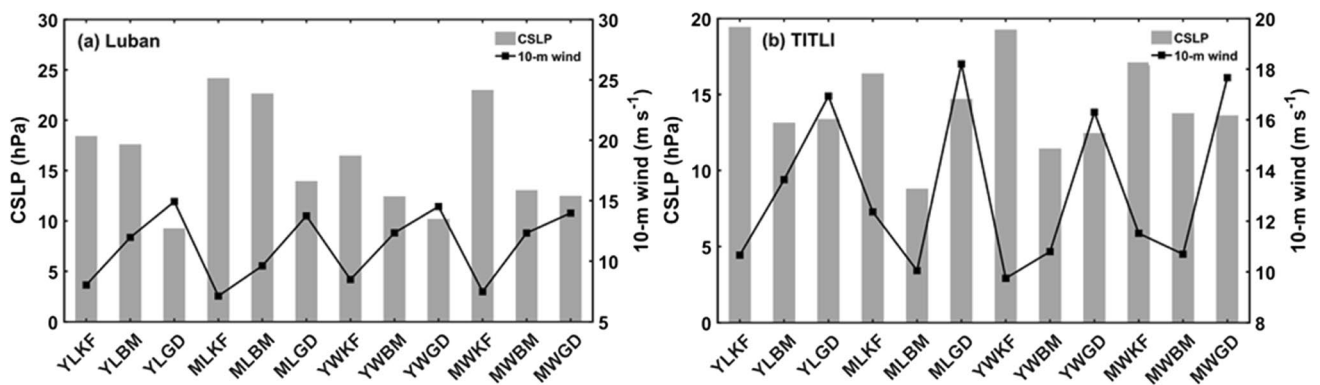

Fig. 5 RMSE of CSLP (hPa; bars) and 10-m wind speed (ms^{-1}; lines) for the different parametrization schemes combinations for (**a**) Luban and (**b**) Titli

and Titli at 00:00 UTC on 11th October. The RMSE for the MWKF is approximately 7.13 ms^{-1} (Fig. 5a), and for the YWKF, it is ~ 9.75 ms^{-1} (Fig. 5b). The combination of BMJ and GD schemes with MYJ and YSU shows that the model is underpredicted the maximum sustained surface wind in the comparison of KF scheme (Fig. 4b,d). The KF scheme has a better ability to emphasize the small-scale features of updraft and downdraft, promoting steady convection

(Kerkhoven et al. 2006; Osuri et al. 2013). BMJ is a convective adjustment scheme; therefore, the predicted convection profile (temperature and moisture) is balanced toward a reference profile in a quasi-equilibrium state because of deep convection. For this situation, the BMJ and GD scheme shows an absence of a low-level convergence, and in this way, diminishing convective activity in the improvement of the cyclonic framework.

Tables 3 and 4 show the CSLP and 10-m wind speed statistics for several studies. The CSLP for Luban shows a low IOA magnitude for all combinations, which is below the acceptable range (0.7 hPa). The MSE, SD, and NMSE for experiment YLGD are 85.76, 6.99, and 5×10^{-6}, respectively. Surface wind for MLKF, on the other hand, shows an IOA of 0.76, which is less than the acceptable range. The MSE (50.81) and NMSE (0.0075) for MLKF, as well as the SD (2.82) for YWKF, are lower than in other experiments (Table 3). Furthermore, for Titli, all combinations except MLBM for CSLP show a lower IOA magnitude than the acceptable range (0.7 hPa). The IOA, MSE, and NMSE for the experiment MLBM are in the range of 0.89, 77.32, and 7×10^{-6}, respectively. The SD for the experiment MLGD is under an acceptable range than others. The MLKF's surface wind suggests an IOA of 0.76, which is below the permissible range. The MSE (50.81), NMSE (0.0075), and SD (2.82) for MLKF and YWKF are lower than in prior studies (Table 4). The aforementioned results show that combining the KF convection scheme with the YSU and MYJ PBL schemes improves surface wind prediction, as proposed by previous studies (Raju et al. 2011; Osuri et al. 2013). However, predicting cyclone track BM convective with both PBL (i.e., MYJ and YSU) schemes has a better ability than the other schemes. Furthermore, the landfall of the cyclones is examined in terms of 24-h accumulated rainfall and statistical measures (e.g., equitable threat score (ETS), bias, percentage correct (PC), false alarm rate (FAR), and the probability of detection (POD)) and is discussed in "Rainfall prediction."

4.2 Rainfall prediction

Figures 6 and 7 illustrate the model simulated 24-h accumulated rainfall for TC Luban and Titli along with GPM observations. The results are in agreement with Mohanty et al. (2010) and indicate that the WRF model is capable enough to simulate rainfall patterns. For TC Luban, the rainfall distribution is well captured by MLBM and very close to the GPM observations. The GD scheme with the combination of YSU and MYJ PBL has failed to predict the rainfall intensity, whereas the KF scheme is overestimated and displaced southward. BMJ CPS with YSU and MYJ PBL simulates the rainfall precisely in view of spatial distribution near the West Bengal and Bangladesh coast. Furthermore, the quantitative rainfall for TC Titli is exaggerated. The simulated rainfall using the KF scheme, on the other hand, is displaced northwards and overestimates the rainfall intensity. The GD scheme fails to reproduce the spatial distribution of precipitation, but in terms of amount, it outperforms with both PBLs (Fig. 7).

The bias and equitable threat score (ETS) for 24-h accumulated rainfall at different thresholds are evaluated to check the ability of individual experiments corresponding to the observed rainfall patterns from GPM, as shown in Fig. 8, and the observed outcomes are reasonably matched with the previous studies (Osuri et al. 2012; Mahala et al. 2019). In the case of Luban, the MLBM experiment has better skill in the prediction of quantitative rainfall with an ETS score > 0.45 at lower threshold (up to 60 mm) (Fig. 8a). The bias of MLBM is > 1 compared with MLKF from the threshold 40 mm onwards, which means the MLBM experiment
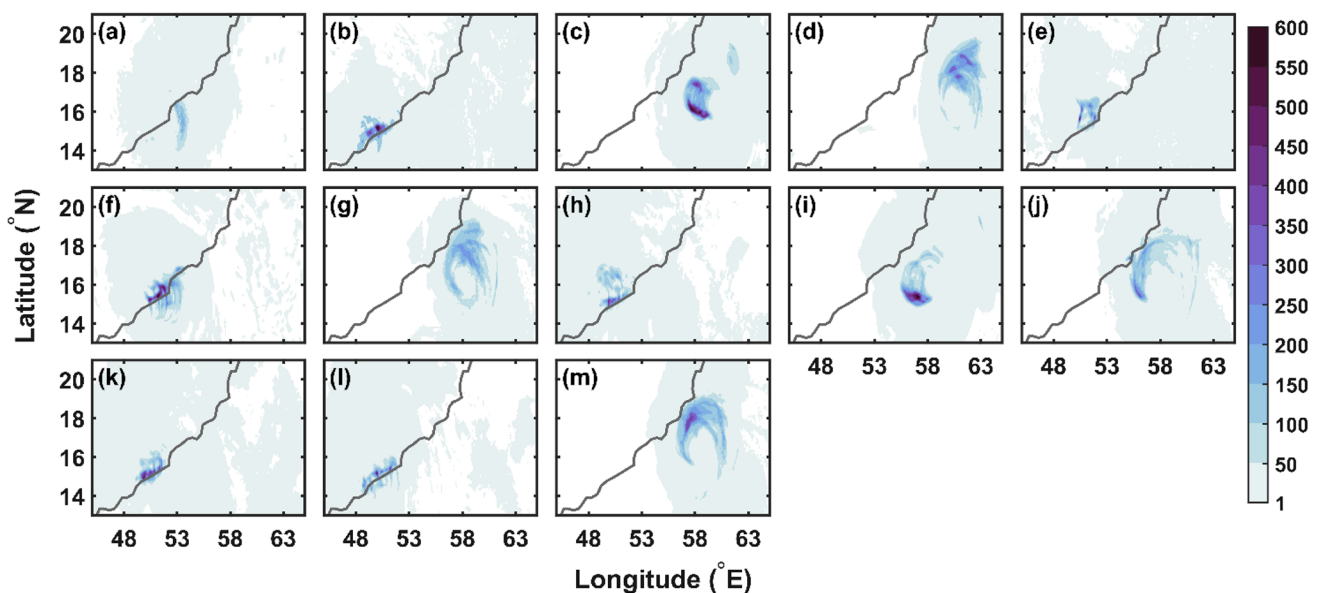

Fig. 6 The spatial distribution of accumulated rainfall (cm) during the landfall of Luban from (**a**) GPM, (**b**) YLKF, (**c**) YLBM, (**d**) YLGD, (**e**) MLKF, (**f**) MLBM, (**g**) MLGD, (**h**) YWKF, (**i**) YWBM, (**j**) YWGD, (**k**) MWKF, (**m**) MWBM, and (**l**) MWGD schemes
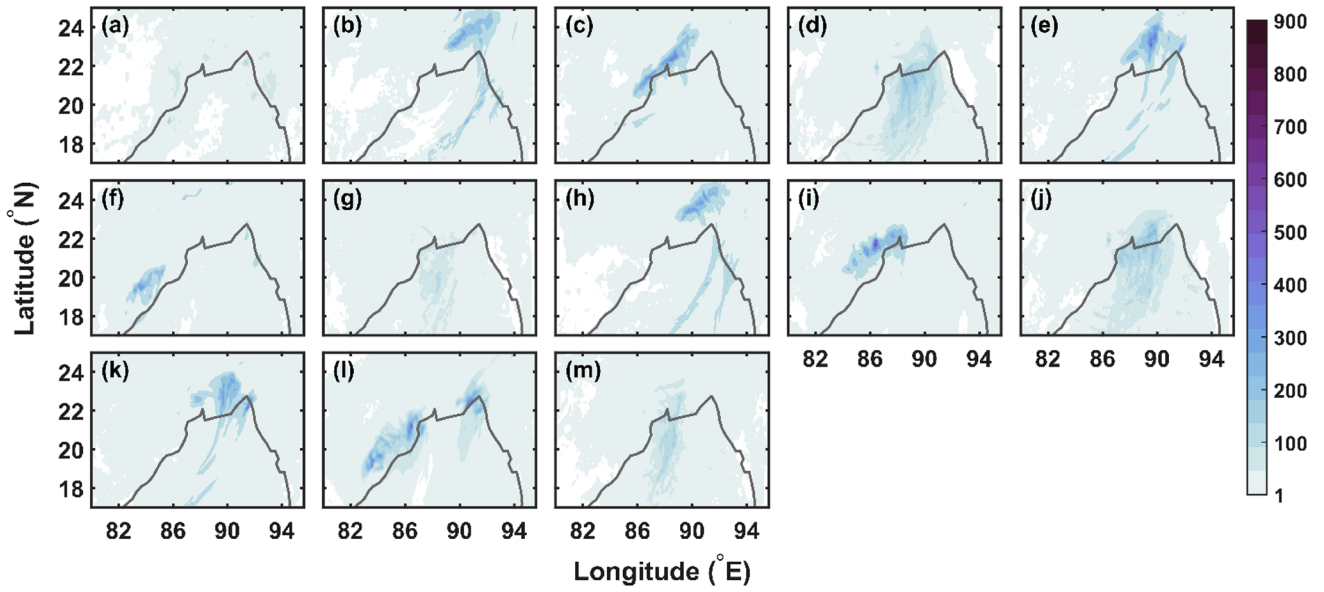
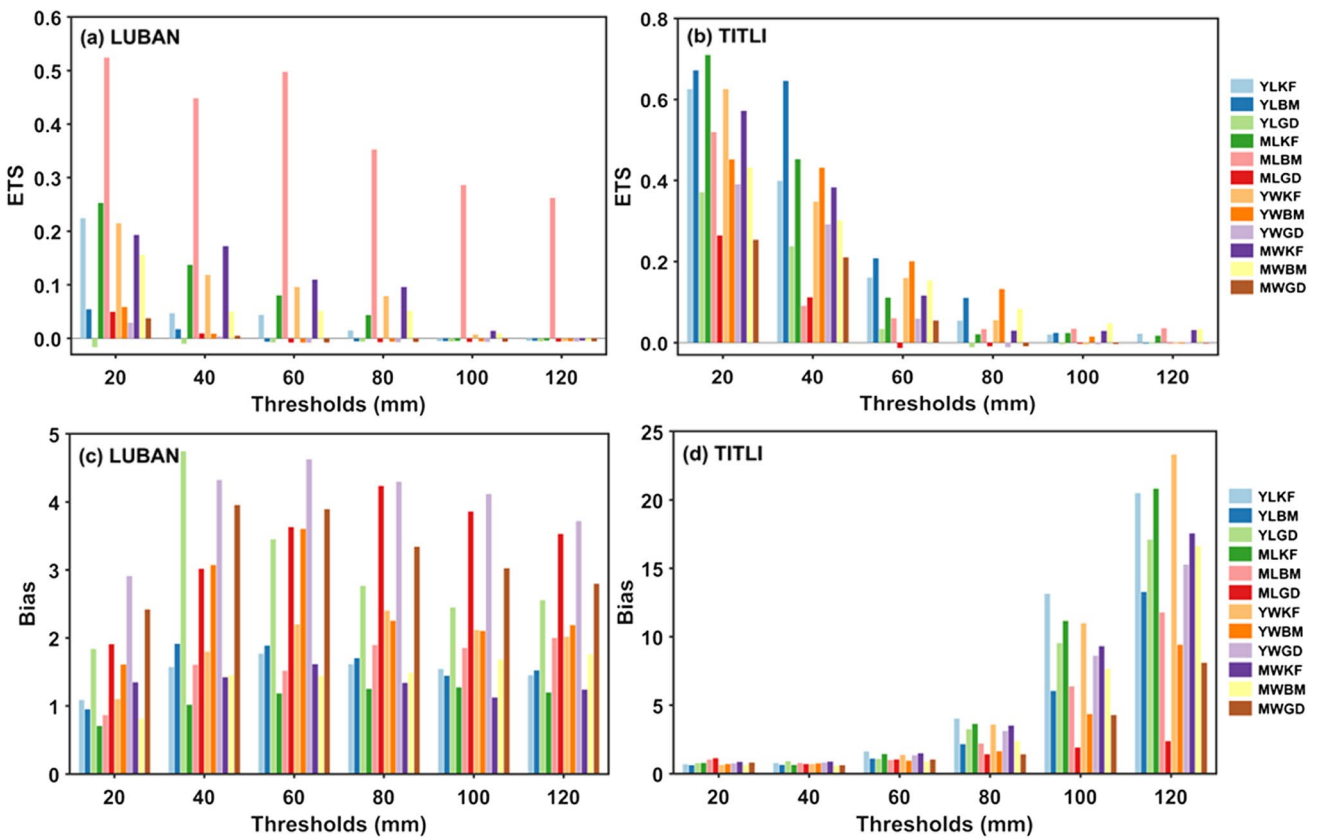**Fig. 7** Same as Fig. 6 but for the Titli

Fig. 8 The equitable threat score (ETS) and bias at different threshold bins for the last 24-h rainfall (i.e., during landfall)

overestimates the rainfall (Fig. 8c). Whereas YLKF, YLBM, MLKF, and YWKF experiment predict the quantitative rainfall well with an ETS score of more than 0.6 at the threshold of 20 mm in the case of Titli. In contrast, the YLBM experiment predicts better rainfall at the threshold of 40 mm and 60 mm with an ETS score of < 6 and < 2, respectively. The YWBM experiment indicates excellent rainfall predictability skills at a higher threshold (from 60 mm onwards) with a higher ETS score than others (Fig. 8b). The bias of YLBM and YWBM schemes are higher (> 1) compared with the MLGD at greater threshold 60 mm onwards, indicating that YLBM and YWBM experiments overestimate the rainfall (Fig. 8d).

Tables 5 and 6 derive statistical performance indices (e.g., PC, FAR, and POD) for rainfall forecast verification at various thresholds. In the case of Luban, MLBM has higher PC skill (nearly 1), lower FAR, and higher POD in the prediction of rainfall at all thresholds (Table 5). At the 20-mm barrier for Titli, the PC for the KF scheme with MYJ is 0.969, but above the 20-mm threshold, the PC for the BMJ convective scheme with the YSU PBL is greater (close to 1). The FAR is lower for the BMJ scheme with the combination of both PBLs, and the POD is higher from the threshold of 80 mm onwards. The values, compared with that similar reported works (Federico et al. 2003, 2008; Avolio and Federico 2018), show a good

Table 5 Statistical performance indexes for the rainfall forecast verification for Luban

	EX	20 mm	40 mm	60 mm	80 mm	100 mm	120 mm
Percent correct (PC)	**YLKF**	0.968	0.972	0.975	0.978	0.978	0.981
	YLBM	0.958	0.967	0.971	0.976	0.979	0.981
	YLGD	0.929	0.931	0.956	0.967	0.971	0.973
	MLKF	0.975	0.982	0.982	0.982	0.981	0.983
	MLBM	**0.986**	**0.988**	**0.992**	**0.988**	**0.987**	**0.987**
	MLGD	0.937	0.954	0.954	0.953	0.959	0.965
	YWKF	0.967	0.974	0.974	0.975	0.974	0.977
	YWBM	0.944	0.953	0.954	0.971	0.974	0.975
	YWGD	0.912	0.938	0.944	0.953	0.957	0.964
	MWKF	0.962	0.980	0.979	0.983	0.983	0.983
	MWBM	0.968	0.974	0.978	0.980	0.978	0.979
	MWGD	0.924	0.942	0.951	0.961	0.966	0.971
False alarm rate (FAR)	**YLKF**	0.633	0.916	0.925	0.968	1.000	1.000
	YLBM	0.872	0.963	1.000	1.000	1.000	1.000
	YLGD	1.000	1.000	1.000	1.000	1.000	1.000
	MLKF	0.496	0.751	0.855	0.917	1.000	1.000
	MLBM	**0.251**	**0.493**	**0.445**	**0.598**	**0.653**	**0.684**
	MLGD	0.906	0.976	1.000	1.000	1.000	1.000
	YWKF	0.647	0.826	0.864	0.889	0.982	1.000
	YWBM	0.888	0.977	1.000	1.000	1.000	1.000
	YWGD	0.938	0.983	1.000	1.000	1.000	1.000
	MWKF	0.701	0.741	0.832	0.840	0.966	1.000
	MWBM	0.682	0.909	0.908	0.910	0.977	1.000
	MWGD	0.926	0.982	1.000	1.000	1.000	1.000
Probability of detection (POD)	**YLKF**	0.399	0.132	0.132	0.052	0.000	0.000
	YLBM	0.122	0.071	0.000	0.000	0.000	0.000
	YLGD	0.000	0.000	0.000	0.000	0.000	0.000
	MLKF	0.354	0.253	0.172	0.104	0.000	0.000
	MLBM	**0.648**	**0.813**	**0.841**	**0.763**	**0.643**	**0.632**
	MLGD	0.180	0.071	0.000	0.000	0.000	0.000
	YWKF	0.389	0.313	0.298	0.267	0.039	0.000
	YWBM	0.180	0.071	0.000	0.000	0.000	0.000
	YWGD	0.180	0.071	0.000	0.000	0.000	0.000
	MWKF	0.402	0.368	0.272	0.215	0.039	0.000
	MWBM	0.259	0.132	0.132	0.133	0.039	0.000
	MWGD	0.180	0.071	0.000	0.000	0.000	0.000

Table 6 Same as Table 5 but for Titli

	EX	20 mm	40 mm	60 mm	80 mm	100 mm	120 mm
Percent correct (PC)	YLKF	0.960	0.940	0.923	0.936	0.944	0.964
	YLBM	0.967	**0.972**	0.944	0.964	0.972	0.975
	YLGD	0.918	0.908	0.921	0.939	0.956	0.968
	MLKF	**0.969**	0.951	0.921	0.937	0.952	0.963
	MLBM	0.936	0.884	0.927	0.958	0.972	0.979
	MLGD	0.877	0.893	0.915	0.965	0.988	**0.994**
	YWKF	0.961	0.935	0.930	0.942	0.950	0.957
	YWBM	0.934	0.946	**0.947**	**0.971**	**0.979**	0.982
	YWGD	0.922	0.923	0.916	0.940	0.960	0.971
	MWKF	0.949	0.935	0.920	0.940	0.960	0.969
	MWBM	0.934	0.933	0.943	0.960	0.967	0.971
	MWGD	0.892	0.917	0.926	0.965	0.978	0.984
False alarm rate (FAR)	YLKF	0.023	0.308	0.745	0.923	0.975	0.976
	YLBM	**0.001**	**0.028**	0.643	0.843	0.968	1.000
	YLGD	0.322	0.545	0.897	1.000	1.000	1.000
	MLKF	0.028	0.163	0.796	0.960	0.971	0.980
	MLBM	0.289	0.738	0.848	0.940	0.958	**0.961**
	MLGD	0.540	0.688	0.982	1.000	1.000	1.000
	YWKF	0.006	0.329	0.731	0.920	1.000	1.000
	YWBM	0.204	0.256	**0.625**	**0.801**	0.978	1.000
	YWGD	0.296	0.445	0.864	1.000	1.000	1.000
	MWKF	0.181	0.366	0.792	0.950	0.965	0.966
	MWBM	0.173	0.320	0.684	0.879	**0.945**	0.964
	MWGD	0.477	0.484	0.859	1.000	1.000	1.000
Probability of detection (POD)	YLKF	0.664	0.532	**0.411**	0.309	0.327	0.500
	YLBM	0.661	**0.653**	0.393	**0.337**	0.192	0.000
	YLGD	0.516	0.414	0.110	0.000	0.000	0.000
	MLKF	**0.750**	0.528	0.292	0.144	0.327	0.409
	MLBM	0.728	0.202	0.151	0.133	0.269	0.455
	MLGD	0.519	0.218	0.019	0.000	0.000	0.000
	YWKF	0.650	0.466	0.368	0.287	0.000	0.000
	YWBM	0.560	0.548	0.350	0.326	0.096	0.000
	YWGD	0.530	0.444	0.181	0.000	0.000	0.000
	MWKF	0.701	0.550	0.308	0.177	0.327	0.593
	MWBM	0.519	0.391	0.277	0.287	**0.423**	**0.591**
	MWGD	0.417	0.313	0.144	0.000	0.000	0.000

performance of WRF simulations. The above result illustrates that the combination of BMJ convective with YSU and MYJ PBL scheme can better predict the rainfall distribution. Furthermore, the TC structure is analyzed to understand the dynamical and thermodynamical aspects, as discussed in "Structure of the tropical cyclones."

4.3 Structure of the tropical cyclones

The longitudinal cross-section of horizontal wind speed (ms^{-1}) along with the cyclone center for all the experiments is presented in Figs. 9 and 10. The KF-YSU and KF-MYJ combination indicates a steady rising motion (45 ms^{-1}) extended up to 100 hPa from the surface in the east–west plane around the storm center in the case of Luban. Moreover, the KF scheme demonstrates the well-defined TC core region and GD convection with YSU and MYJ presented weak rising motion (25 ms^{-1}) and described the cyclone's worst eyewall (Fig. 9). The same results have been observed in the case of the TC Titli. The KF convection shows a steady rising motion (25 ms^{-1}) extended up to 200 hPa from the surface in the east–west plane around the storm center.
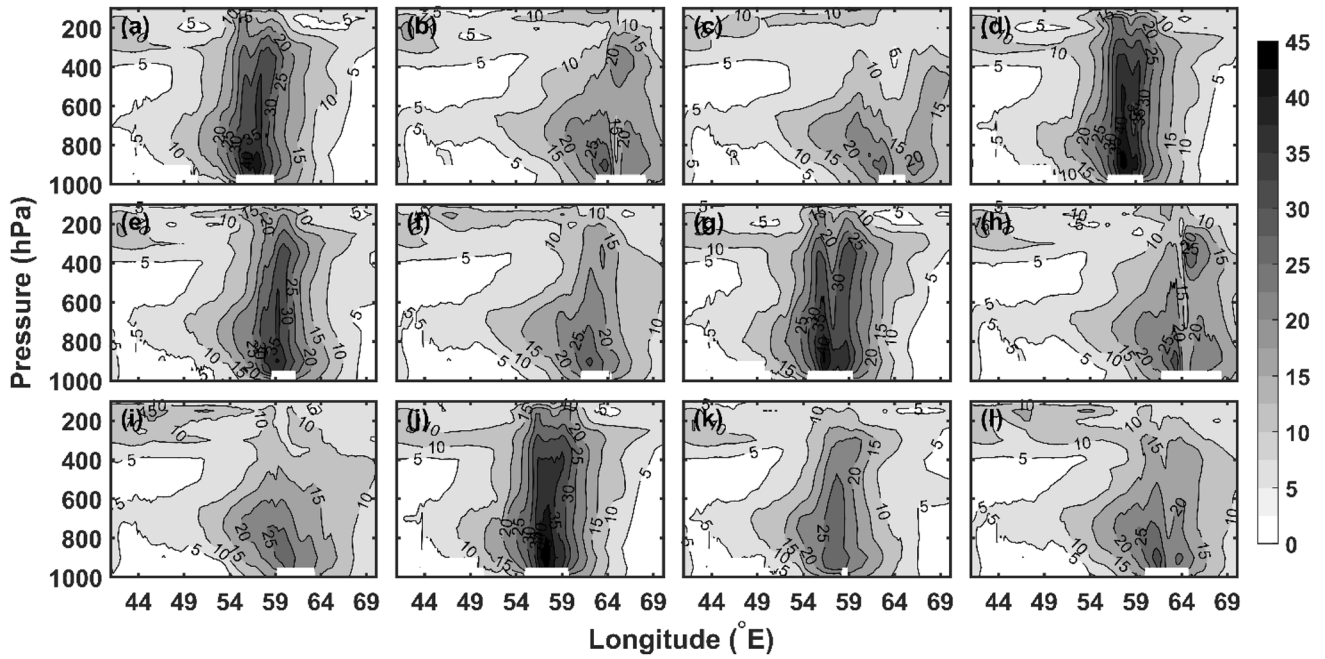
Fig. 9 The spatial distribution of east–west cross-section horizontal wind speed (ms^{-1}) through the center of Luban from different experiments: (**a**) YLKF, (**b**) YLBM, (**c**) YLGD, (**d**) MLKF, (**e**) MLBM, (**f**) MLGD, (**g**) YWKF, (**h**) YWBM, (**i**) YWGD, (**j**) MWKF, (**k**) MWBM, and (**l**) MWGD
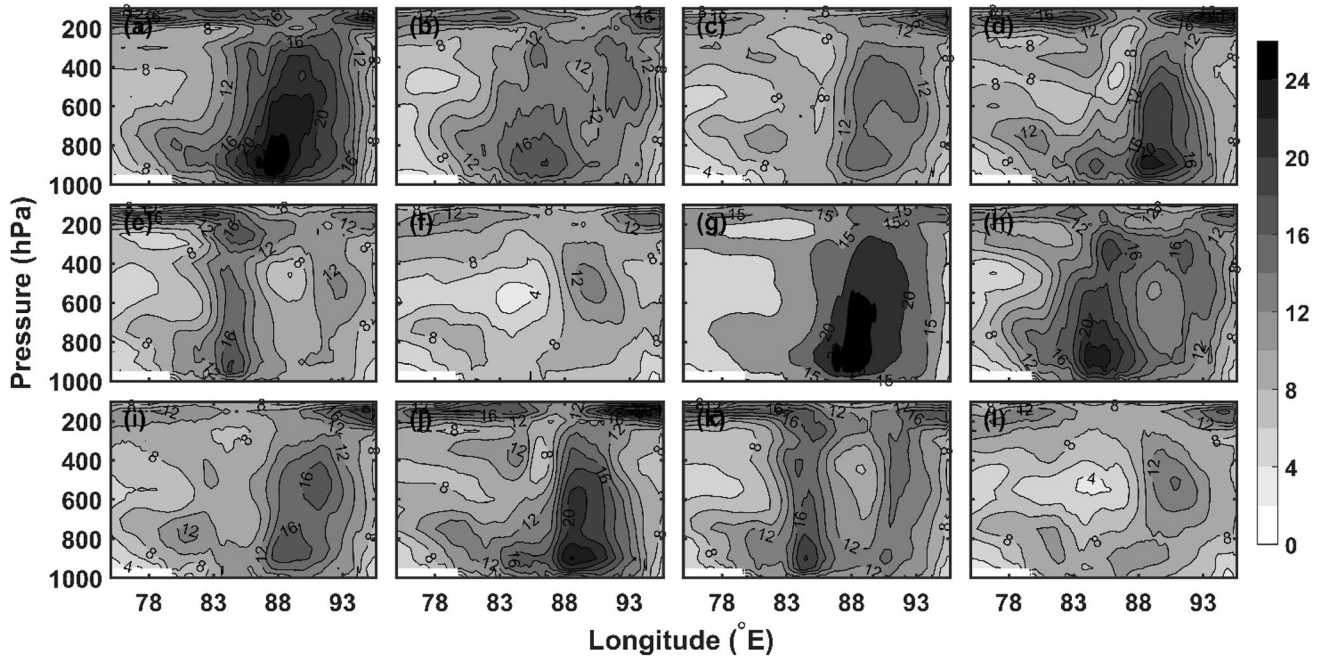

Fig. 10 Same as Fig. 9 but for the Titli

The KF convective demonstrates a well-defined eyewall, and on the other hand, GD convection with YSU and MYJ represented weak rising motion (16 ms^{-1}) and described the worst eyewall (Fig. 10). The results show that the KF scheme

allows for deep convection in the air column with robust updraft and downdraft. In both cyclonic cases, all the BMJ and GD scheme simulations with YSU and MYJ are not able to determine the strong updraft except MLBM, as simulated

by the KF scheme. The experiment MLBM shows a maximum rising motion of 35 ms^{-1} for Luban and 16 ms^{-1} in the case of Titli. In terms of intensity, MLBM is not good as KF with YSU and MYJ, but it shows a well-defined eyewall of the cyclone. The results indicate that the KF scheme has a better ability to predict intensity for severe weather conditions such as a TC (Pattanayak and Mohanty 2008).

The vertical profile of equivalent potential temperature (θ_e) for different convection and PBL schemes are shown in Fig. 11. The θ_e is generally used to analyze the thermodynamical progressions in the matured stage (very severe condition) of the TC (Dolling and Barnes 2012). According to Sikora (1976), the incredibly high equivalent potential temperature can signal a phase of subsequent explosive deepening. These characteristics of warm core structures with profound warming are most likely due to the combined effect of the following: (1) large-scale upward surface fluxes of sensible and latent heat from the underlying warm ocean due to strong updrafts in the eye wall region and (2) a significant reduction in cooler penetrative downdrafts due to increased warming tendencies in the TC core (Pattnaik and Krishnamurti 2007). The area-averaged vertical variation is shown over 100 km of radius from the TC eye. KF-YSU and KF-MYJ indicate higher θ_e values and intense vertical mixing throughout the pattern, whereas the GD scheme shows less θ_e value at the surface and mixing taking place up to 500 hPa in the case of Luban (Fig. 11a). Similarly, for TC Titli, results indicate the KF scheme with YSU and MYJ infers high θ_e values and intense vertical mixing up to 400 hPa. However, the GD scheme shows less θ_e values at the surface and vertical mixing is taking place up to 600 hPa (Fig. 11b). The θ_e values of the BMJ scheme with MYJ lie between KF and GD schemes. The result proposes that the boundary layer's illustration is determined more convincingly in both the PBL (YSU and MYJ). Because of the intense vertical propelling of heat, a warmer TC core can form and increase cyclone intensity

(Raju et al. 2011). The combination of the GD scheme with YSU and MYJ PBL shows the surface value of θ_e is less in comparison to the KF scheme, thus reducing the vertical propelling of heat around the system. The overall discussion indicates the model performed well to simulate the cyclone track, intensity, and landfall with the comparison of observational analysis.

5 Conclusion

The twelve experiments with three convection, two PBL, and two microphysical parameterization schemes have been designed to carry out the numerical simulations using the WRF-ARW model to forecast the TC Luban and Titli over the NIO region. The results demonstrate that the convective and PBL scheme controls the cyclone intensity, while the microphysics scheme impacts track prediction. The cyclone intensity is underestimated by the model in view of surface wind and overestimated for central sea level pressure for all sensitivity experiments. The KF convection scheme combined with WDM6 microphysics and MYJ PBL for Luban and YSU PBL for Titli has a better prediction skill of maximum sustained surface wind speed, accounting for RMSE is about 7.13 ms^{-1} for Luban and 9.75 ms^{-1} for Titli. However, The BMJ and GD scheme with the same combination of microphysics and PBL indicates that the RMSE value of maximum sustained surface wind speed is > 10 ms^{-1}, which is more divergent from the actual. Also, the cyclone structure is well captured by MYJ–KF and YSU-KF in both space and time for Luban and Titli, respectively. The MYJ-BMJ combination is well capturing the TC track for Luban and YSU-BMJ for Titli with the WDM6 microphysics scheme. The vector displacement error and RMSE for the experiment MWBM and YWBM are < 100 km and < 10 km, respectively. MYJ-BMJ and YSU-BMJ with the Lin et al.

Fig. 11 The vertical profile of area-averaged equivalent potential temperature (°K) at a 100 km radius from the storm center for (**a**) Luban and (**b**) Titli
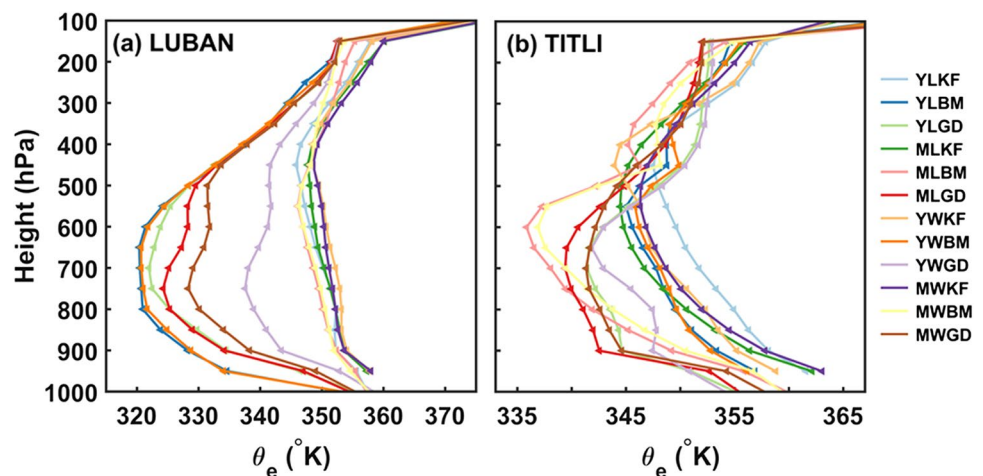
microphysics scheme have better skills for rainfall prediction. The experiment MLBM has an equitable threat score of < 0.45 up to 60 mm, and at the higher threshold, it is < 0.3 up to 120 mm in the case of Luban. The YLBM experiment has an equitable threat score of < 0.6 up to 40 mm, and at 60 mm, it is < 0.2 for the case of Titli. The YWBM shows better predictability at a higher threshold. Overall, the tropical cyclones Luban and Titli's track, intensity, and timing of landfall were accurately predicted by the WRF model, showing that the model has the potential to be used for operational purposes. Additionally, the model could precisely determine the spatial distribution of precipitation.

A precise prediction of cyclone track, intensity, and landfall remains a difficult issue, with much room for improvement through precise vortex relocation, initialization, and incorporation of satellites as well as other accessible information over the open ocean. The primary elements impacting cyclone prediction embrace model resolution, multiple parameterization schemes, and initial conditions including realistic steering flow. Therefore, improved initial conditions and enhanced data assimilation techniques may enable better prediction of tropical storm origin, structure, and intensity.

Appendix 1. Performance indicator for numerical simulations

Each statistical parameter plays a fundamental role in validating numerical simulations and vulnerability estimation, but some of them are essential to consider (Borrego et al. 2008). This study has considered RMSE, IOA, MSE, and SD (Schlünzen and Sokhi 2008; Emery et al. 2001; Gilliam et al. 2006).

Root mean square error

Root mean square error (RMSE) gives the absolute model error between the observed and predicted values characterized as

$$RMSE = \sqrt{\frac{\sum_{i=1}^{N} (P_i - O_i)^2}{N}}$$

Index of agreement

Index of agreement (IOA) is characterized by the match between the departure of each prediction and the departure of each observation from the observed mean and represented as (Willmott 1981)

$$IOA = 1 - \frac{\sum_{i=1}^{N} (O_i - P_i)^2}{\sum_{i=1}^{N} \left(\left| P_i - \overline{O} \right| + \left| O_i - \overline{O} \right| \right)^2}$$

Here, O_i and P_i are represented by observed and predicted data. However, O and P are defined by the observed mean and predicted mean, respectively. Theoretically, the IOA varies between 0 and 1, where 1 is a perfect match and 0 is no match between predicted and observed values.

Mean square error

Mean square error (MSE) is a proportion of the mean squared difference between the predicted and observed values characterized as

$$MSE = \frac{1}{N} \sum_{i=1}^{N} (P_i - O_i)^2$$

The MSE values are always positive, and those closer to zero are better.

Standard deviation

Standard deviation (SD) is a measure of the spread of the individual modeled values from the mean of the modeled values defined as

$$\sigma = \sqrt{\frac{1}{N} \sum_{i=1}^{N} \left(M_i - \overline{M} \right)^2}$$

Normalized mean square error

Normalized mean square error (NMSE) is a measure of the overall deviations between predicted and observed values, defined as

$$NMSE = \frac{1}{N} \sum_{i=1}^{N} \frac{(P_i - O_i)^2}{\overline{PO}}$$

The low NMSE shows that the model is performing well in both space and time. In contrast, a high NMSE value does not imply that the model is completely wrong. That could be due to shifting in time and space.

Appendix 2. Forecast verification methods

For the validation of rainfall, standard verification methods are used and discussed below.

		Observed		
		Yes	No	Total
Forecast	**Yes**	H	FA	Forecast yes
	No	M	CN	Forecast no
Total		Observed yes	Observed no	Total

Here, "H" implies the event that is forecast to happen, and happened, i.e., hits, "M" implies the event that is forecast not to happen, but happened, i.e., misses, and "FA" implies the event that is forecast to happen, however, did not happen, i.e., false alarm, and "CN" implies the event that forecast not to happen and did not happen, i.e., correct negatives.

Equitable threat score

Equitable threat score (ETS) is characterized by the ratio of observed and/or forecast event that was correctly predicted after removing the random hits R_H which is associated by chance and described as

$$ETS = \frac{H - R_H}{H + M + FA - R_H}$$

$$R_{hits} = \frac{(H + M)(H + FA)}{total}$$

ETS varies between $-1/3$ and 1, where 1 indicates a perfect score and 0 represents no skill.

Percentage correct

Percentage correct (PC) is the fraction of correct events and the total no of events.

$$PC = \frac{H + CN}{H + M + FA + CN}$$

PC varies between 0 and 1, where 1 indicates a perfect score and 0 has no skill to produce a forecast.

False alarm rate

False alarm rate (FAR) is defined as the fraction of events that did not occur, and the number of events is forecasted.

$$FAR = \frac{FA}{H + FA}$$

The smaller value of FAR indicates better skill and varies between 0 and 1. The perfect score is equal to 0, while 1 shows no skill.

Probability of detection

Probability of detection (POD) is characterized by the ratio of observed "yes" events which are predicted accurately (hits) and the number of observed "yes" events (misses), represented by

$$POD = \frac{H}{H + M}$$

POD varies between 0 and 1, where 1 is the perfect score.

Author contribution Conceptualization, methodology, and investigation: Saurabh Verma; writing original draft preparation: Saurabh Verma, Subodh Kumar, and Sunny Kant; writing, review, and editing: Sunny Kant, Sanchit Mehta, Saurabh Verma, and Subodh Kumar.

Data availability Data is available upon request to the corresponding author.

Code availability All the plots are made using MATLAB, and the code is available upon request.

Declarations

Ethics approval All authors comply with the guidelines of the journal Theoretical and Applied Climatology.

Consent to participate All authors agreed to participate in this study.

Consent for publication The authors agree to the publication of this study.

Conflict of interest The authors declare no competing interests.

References

Avolio E, Federico S (2018) WRF simulations for a heavy rainfall event in southern Italy: verification and sensitivity tests. Atmos Res 209:14–35. https://doi.org/10.1016/j.atmosres.2018.03.009

Baki H, Balaji C, Srinivasan B (2022) Impact of data assimilation on a calibrated WRF model for the prediction of tropical cyclones over the Bay of Bengal. Curr Sci 122(5):569

Balaji M, Chakraborty A, Mandal M (2018) Changes in tropical cyclone activity in north Indian Ocean during satellite era (1981–2014). Int J Climatol 38(6):2819–2837

Bender MA, Ginis I (2000) Real-case simulations of hurricane–ocean interaction using a high-resolution coupled model: effects on hurricane intensity. Mon Weather Rev 128(4):917–946. https://

doi.org/10.1175/1520-0493(2000)128%3c0917:RCSOHO%3e2.0.CO;2

Betts AK, Miller MJ (1986) A new convective adjustment scheme. Part II: single column tests using GATE wave, BOMEX, ATEX and arctic air-mass data sets. Q J Royal Meteorol Soc 112(473):693–709. https://doi.org/10.1002/qj.49711247308

Borrego C, Monteiro A, Ferreira J, Miranda AI, Costa AM, Carvalho AC, Lopes M (2008) Procedures for estimation of modelling uncertainty in air quality assessment. Environ Int 34(5):613–620. https://doi.org/10.1016/j.envint.2007.12.005

Chandrasekar R, Balaji C (2012) Sensitivity of tropical cyclone Jal simulations to physics parameterizations. J Earth Syst Sci 121(4):923–946

De Maria W (2005) Whistleblower protection: is Africa ready? Public Adm Dev 25(3):217–226. https://doi.org/10.1002/pad.343

Deshpande MS, Pattnaik S, Salvekar PS (2012) Impact of cloud parameterization on the numerical simulation of a super cyclone. In Annales Geophysicae 30(5):775–795. Copernicus GmbH.

Dolling KP, Barnes GM (2012) The creation of a high equivalent potential temperature reservoir in Tropical Storm Humberto (2001) and its possible role in storm deepening. Mon Weather Rev 140(2):492–505. https://doi.org/10.1175/MWR-D-11-00068.1

Emery C, Tai E, Yarwood G (2001) Enhanced meteorological modeling and performance evaluation for two Texasozone episodes, Technical Report, Texas Natural Resource Conservation Commission, ENVIRON InternationalCorporation, Work Assignment No. 31984-11, Environ International Corporation, Novato, pp 235

Federico S, Bellecci C, Colacino M (2003) Numerical simulation of Crotone flood: storm evolution. Il Nuovo Cimento C 26(4):357–371

Federico S, Avolio E, Bellecci C, Lavagnini A, Colacino M, Walko RL (2008) Numerical analysis of an intense rainstorm occurred in southern Italy. Nat Hazard 8(1):19–35. https://doi.org/10.5194/nhess-8-19-2008,2008

Gilliam RC, Hogrefe C, Rao ST (2006) New methods for evaluating meteorological models used in air quality applications. Atmos Environ 40(26):5073–5086. https://doi.org/10.1016/j.atmosenv.2006.01.023

Grell GA, Dévényi D (2002) A generalized approach to parameterizing convection combining ensemble and data assimilation techniques. Geophys Res Lett 29(14):38–41. https://doi.org/10.1029/2002GL015311

Gunwani P, Mohan M (2017) Sensitivity of WRF model estimates to various PBL parameterizations in different climatic zones over India. Atmos Res 194:43–65. https://doi.org/10.1016/j.atmosres.2017.04.026

Hon KK (2020) Tropical cyclone track prediction using a large-area WRF model at the Hong Kong Observatory. Trop Cyclone Res Rev 9(1):67–74. https://doi.org/10.1016/j.tcrr.2020.03.002

Hong SY, Lim JOJ (2006) The WRF single-moment 6-class microphysics scheme (WSM6). Asia-Pac J Atmos Sci 42(2):129–151

Hong SY, Pan HL (1996) Nonlocal boundary layer vertical diffusion in a medium-range forecast model. Mon Weather Rev 124(10):2322–2339. https://doi.org/10.1175/1520-0493(1996)124%3c2322:NBLVDI%3e2.0.CO;2

IMD annual report (2018) A very severe cyclonic storm 'LUBAN' over the Arabian Sea (06 – 15 October 2018); https://metnet.imd.gov.in/imdnews/ar2018.pdf

Janjić ZI (1994) The step-mountain eta coordinate model: further developments of the convection, viscous sublayer, and turbulence closure schemes. Mon Weather Rev 122(5):927–945. https://doi.org/10.1175/15200493(1994)122%3c0927:TSMECM%3e2.0.CO;2

JTWC annual report (2018) A very severe cyclonic storm 'LUBAN' over the Arabian Sea (06 – 15 October 2018); https://www.metoc.navy.mil/jtwc/products/atcr/2018atcr.pdf

Kain JS, Fritsch JM (1993) Convective parameterization for mesoscale models: the Kain-Fritsch scheme. In The representation of cumulus convection in numerical models 165–170. Am Meteorol Soc, Boston, MA. https://doi.org/10.1007/978-1-935704-13-3_16

Kanase RD, Salvekar PS (2015) Impact of physical parameterization schemes on track and intensity of severe cyclonic storms in Bay of Bengal. Meteorol Atmos Phys 127(5):537–559

Kerkhoven E, Gan TY, Shiiba M, Reuter G, Tanaka K (2006) A comparison of cumulus parameterization schemes in a numerical weather prediction model for a monsoon rainfall event. Hydrol Process: Int J 20(9):1961–1978. https://doi.org/10.1002/hyp.5967

Knaff JA, DeMaria M, Sampson CR, Gross JM (2003) Statistical, 5-day tropical cyclone intensity forecasts derived from climatology and persistence. Weather Forecast 18(1):80–92. https://doi.org/10.1175/1520-0434(2003)018%3c0080:SDTCIF%3e2.0.CO;2

Krishnamurti TN, Pattnaik S, Stefanova L, Kumar TV, Mackey BP, O'shay AJ, Pasch RJ (2005) The hurricane intensity issue. Mon Weather Rev 133(7):1886–1912. https://doi.org/10.1175/MWR2954.1

Lin YL, Farley RD, Orville HD (1983) Bulk parameterization of the snow field in a cloud model. J Appl Meteorol Climatol 22(6):1065–1092. https://doi.org/10.1175/1520-0450(1983)022%3c1065:BPOTSF%3e2.0.CO;2

Mahala BK, Mohanty PK, Das M, Routray A (2019) Performance assessment of WRF model in simulating the very severe cyclonic storm "TITLI" in the Bay of Bengal: a case study. Dyn Atmos Oceans 88:101106. https://doi.org/10.1016/j.dynatmoce.2019.101106

Makar P, Pant V (2022) Numerical simulations of tropical cyclones Amphan and Nisarga with incorporation of sea surface temperature in the model. In OCEANS 2022, IEEE, Chennai, pp 1–6

Mandal M, Mohanty UC, Raman S (2004) A study on the impact of parameterization of physical processes on prediction of tropical cyclones over the Bay of Bengal with NCAR/PSU mesoscale model. Nat Hazards 31(2):391–414

Mohan PR, Srinivas CV, Yesubabu V, Baskaran R, Venkatraman B (2019) Tropical cyclone simulations over Bay of Bengal with ARW model: sensitivity to cloud microphysics schemes. Atmos Res 230:104651

Mohandas S, Ashrit R (2014) Sensitivity of different convective parameterization schemes on tropical cyclone prediction using a mesoscale model. Nat Hazards 73(2):213–235

Mohanty UC, Akhilesh G (1997) Deterministic methods for prediction of very severe cyclonic storm tracks. Mausam 48:257–272

Mohanty UC, Osuri KK, Routray A, Mohapatra M, Pattanayak S (2010) Simulation of Bay of Bengal tropical cyclones with WRF model: Impact of initial and boundary conditions. Mar Geodesy 33(4):294–314. https://doi.org/10.1080/01490419.2010.518061

Mohanty UC, Osuri KK, Pattanayak S, Sinha P (2012) An observational perspective on tropical cyclone activity over Indian seas in a warming environment. Nat Hazards 63:1319–1335. https://doi.org/10.1007/s11069-011-9810-z

Mohanty S, Nadimpalli R, Osuri KK, Pattanayak S, Mohanty UC, Sil S (2019) Role of sea surface temperature in modulating life cycle of tropical cyclones over Bay of Bengal. Trop Cyclone Res Rev 8(2):68–83. https://doi.org/10.1016/j.tcrr.2019.07.007

Mohapatra M, Geetha B, Balachandran S, Rathore LS (2015) On the tropical cyclone activity and associated environmental features over North Indian Ocean in the context of climate change. J Clim Change 1(1, 2):1–26.

Osuri KK, Mohanty UC, Routray A, Kulkarni MA, Mohapatra M (2012) Customization of WRF-ARW model with physical parameterization schemes for the simulation of tropical cyclones over North Indian Ocean. Nat Hazards 63(3):1337–1359

Osuri KK, Mohanty UC, Routray A, Mohapatra M, Niyogi D (2013) Real-time track prediction of tropical cyclones over the North Indian Ocean using the ARW model. J Appl Meteorol Climatol 52(11):2476–2492

Pattanayak S, Mohanty UC (2008) A comparative study on performance of MM5 and WRF models in simulation of tropical cyclones over Indian seas. Curr Sci 95(7):923–936

Pattanayak S, Mohanty UC, Osuri KK (2012) Impact of parameterization of physical processes on simulation of track and intensity of tropical cyclone Nargis (2008) with WRF-NMM model. Sci World J. https://doi.org/10.1100/2012/671437

Pattnaik S, Krishnamurti TN (2007) Impact of cloud microphysical processes on hurricane intensity, part 2: Sensitivity experiments. Meteorol Atmos Phys 97(1):127–147. https://doi.org/10.1007/s00703-006-0248-x

Raju PVS, Potty J, Mohanty UC (2011) Sensitivity of physical parameterizations on prediction of tropical cyclone Nargis over the Bay of Bengal using WRF model. Meteorol Atmos Phys 113:125–137

Ramage CS (1974) Monsoonal influences on the annual variation of tropical cyclone development over the Indian and Pacific Oceans. Mon Weather Rev 102(11):745–753

Rao DB, Prasad DH (2007) Sensitivity of tropical cyclone intensification to boundary layer and convective processes. Nat Hazards 41(3):429–445

Rao GV, Rao DB (2003) A review of some observed mesoscale characteristics of tropical cyclones and some preliminary numerical simulations of their kinematic features. Proc-Indian National Sci Acad Part A 69(5):523–542

Rogers R, Aberson S, Black M, Black P, Cione J, Dodge P, Shay N (2006) The intensity forecasting experiment: a NOAA multiyear field program for improving tropical cyclone intensity forecasts. Bull Am Meteor Soc 87(11):1523–1538. https://doi.org/10.1175/BAMS-87-11-1523

Roy Chowdhury R, Kumar SP, Chakraborty A (2021) The role of mixed Rossby gravity wave and initiation of MJO propagation for the triggering of simultaneous cyclones over North Indian Ocean in October 2018 and associated upper ocean responses. In AGU Fall Meet Abstr 2021:A25R-1911

RSMC—Tropical Cyclone (2019) In report on cyclonic disturbances over the North Indian Ocean during 2018; Government of India, New Delhi

Rutledge SA, Hobbs PV (1984) The mesoscale and microscale structure of organization of clouds and precipitation in midlatitude cyclones. XII: a diagnostic modeling study of precipitation development in narrow cold-frontal rainbands. J Atmos Sci 41:2949–2972. https://doi.org/10.1175/1520-0469(1984)041%3c2949:TMAMSA%3e2.0.CO;2

Schlünzen KH, Sokhi RS (2008) Overview of tools and methods for meteorological and air pollution mesoscale model evaluation and user training. Joint Report WMO COST 728:116

Sikora CR (1976) An investigation of equivalent potential temperature as a measure of tropical cyclone intensity. Fleet Weather Central/Joint Typhoon Warning Center Fpo San Francisco. https://apps.dtic.mil/sti/pdfs/ADA064520.pdf

Skamarock WC, Klemp J B, Dudhia J, Gill DO, Barker DM, Wang W, Powers JG (2005) A description of the advanced research WRF version 2 (No. NCAR/TN-468+ STR). National Center for Atmospheric Research Boulder Co Mesoscale and Microscale Meteorology Div.

Skamarock WC, Klemp JB (1992) The stability of time-split numerical methods for the hydrostatic and the nonhydrostatic elastic equations. Mon Weather Rev 120(9):2109–2127. https://doi.org/10.1175/1520-0493(1992)120%3c2109:TSOTSN%3e2.0.CO;2

Skamarock WC, Klemp JB, Dudhia J, Gill DO, Liu Z, Berner J et al (2019) A description of the advanced research WRF model version 4. National Center for Atmospheric Research: Boulder, CO, USA 145:145. https://doi.org/10.5065/1dfh-6p97

Srinivas CV, Bhaskar Rao D, Yesubabu V, Baskaran R, Venkatraman B (2013) Tropical cyclone predictions over the Bay of Bengal using the high-resolution Advanced Research Weather Research and Forecasting (ARW) model. Q J R Meteorol Soc 139(676):1810–1825

Srivastava A, Prasad VS, Das AK, Sharma A (2021) A HWRF-POM-TC coupled model forecast performance over North Indian Ocean: VSCS TITLI & VSCS LUBAN. Trop Cyclone Res Rev 10(1):54–70

Sun Y, Zhong Z, Lu W, Hu Y (2014) Why are tropical cyclone tracks over the western North Pacific sensitive to the cumulus parameterization scheme in regional climate modeling? A case study for Megi (2010). Mon Weather Rev 142(3):1240–1249

Vishnu S, Sanjay J, Krishnan R (2019) Assessment of climatological tropical cyclone activity over the north Indian Ocean in the CORDEX-South Asia regional climate models. Clim Dyn 53(7):5101–5118

Wang W, Barker D, Bruyere C, Dudhia J, Gill D, Michalakes J (2004) WRF version 2 modeling system user's guide. Available at: http://www.mmm.ucar.edu/wrf/users/docs/user.guide/. Accessed May 2021

Willmott CJ (1981) On the validation of models. Phys Geogr 2:184–194. https://doi.org/10.1080/02723646.1981.10642213

WMO (2014) Tropical cyclone operational plan for the Bay of Bengal and the Arabian Sea. Available at: http://www.wmo.int/pages/prog/www/tcp/operational-plans.html.

Publisher's note Springer Nature remains neutral with regard to jurisdictional claims in published maps and institutional affiliations.